 doi:10.20944/preprints202207.0265.v1

Article

Early Detection of Wildfires with GOES-R Time Series and Deep GRU-Network

Yu Zhao [1], and Yifang Ban [1]*

[1] Affiliation 1; Division of Geoinformatics, KTH Royal Institute of Technology
* Correspondence: yifang@kth.se; Tel.: +46-08-790 8648
† Current address: Teknikringen 10A, Sweden.

Abstract: Early detection of wildfires has been limited using the sun-synchronous orbit satellites due to their low temporal resolution and wildfires' fast spread in the early stage. NOAA's geostationary weather satellites GOES-R can acquire images every 15 minutes at 2km spatial resolution, and have been used for early fire detection. However, advanced processing algorithms are needed to provide timely and reliable detection of wildfires. In this research, a deep learning framework, based on Gated Recurrent Units (GRU), is proposed to detect wildfires at early stage using GOES-R dense time series data. GRU model maintains good performance on temporal modelling while keep a simple architecture, makes it suitable to efficiently process time-series data. 36 different wildfires in North and South America under the coverage of GOES-R satellites are selected to assess the effectiveness of the GRU method. The detection times based on GOES-R are compared with VIIRS active fire products at 375m resolution in NASA's Fire Information for Resource Management System (FIRMS). The results show that GRU-based GOES-R detections of the wildfires are earlier than that of the VIIRS active fire products in most of the study areas. Also, results from proposed method offer more precise location on the active fire at early stage than GOES-R Active Fire Product in mid-latitude and low-latitude regions.

Keywords: GOES-R; GRU; Deep Learning; Wildfires; Active Fires; Early Detection; Monitoring

1. Introduction

In recent years, climate change and human activities have caused increasing numbers of wildfires. At the same time, both of the frequency and severity of wildfires are expected to increase due to climate change[1]. In 2021, California had 8835 incidents that burned a total of 1,039,616 hectares while British Columbia had 1610 wildfires that burned 868,203 hectares. While in California, in 2021, there has been 8835 incidents and total 1,039,616 hectares of land burned. Among those most hazardous wildfires, the spreading speed for some of them is extremely high. For example, Dixie Fire in 2021 spreaded very fast in first several days because of the strong winds. Therefore, early detection of the active fire has become increasingly important to support early response and suppression efforts, thus reduce the damages caused by the fast-spreading wildfires.

Several early fire detection systems have been developed using remote sensing technologies, including satellite-based system, aerial based system and terresterial-based system. It is believed that such system can mitigate the impact of the wildfires in early stages [2]. Pasty studies have explored the use of satellite images for active fire detection. Using medium-resolution satellite data, Hu et al. [3] evaluated Sentinel-2 images for active fire detection. In [4] and [5], Landsat-8 images were exploited to detect active fires. However, low temporal resolution of Sentinel-2 and Landsat-8 data offer very limited capability for active fire detection due to their low temporal resolution.

Using coarse resolution data from sun-synchronous orbit satellites, a number of active fire products have been developed to provide the location and the time of the active fires on a daily basis [6][7][8]. Visible Infrared Imaging Radiometer Suite (VIIRS) [6] on board Suomi

National Polar-orbiting Partnership (NPP) satellite, Sea and Land Surface Temperature Radiometer (SLSTR) on board Sentinel-3 satellite and the Moderate Resolution Imaging Spectroradiometer (MODIS) [7] on board Terra and Aqua are among the most commonly used instruments to detect active fire points. MODIS active fire product(MCD14DL) and VIIRS active fire product(VNP14IMG) both offer day and night observations of active fire pixels, owing to the revisit time of roughly half a day. In terms of spatial resolution, VIIRS active fire product offers 375m spatial resolution while MODIS active fire product offers 1 km spatial resolution [9][10]. Higher spatial resolution of VIIRS sensor helps to detect more active fire pixels as high spatial resolution helps to detect low-intensity fires [11]. Sentinel-3 SLSTR has similar capture time and spatial resolution as MODIS, but in [8], the author argued that SLSTR can detect fires with lower FRP than MODIS, where fire radiance power(FRP) is used to quantify fire intensity and fire severity [12]. However, revisit time of half a day is still not sufficient for early fire detection, given the fact that some wildfires spread swiftly in the early stage.

Hence, the need for higher temporal resolution motivates the emerging of active fire product using geostationary satellites like Geostationary Operational Environmental Satellites R Series(GOES-R). GOES-R series, consists of 2 geostationary satellites, GOES-16 and GOES-17, can provide the full coverage of North America and South America. At the same time, owing to the high temporal resolution of GOES-R satellites, each image is acquired every 15 minutes.

In [13][14], GOES Early Fire Detection (GOES-EFD) utilizing images from GOES satellites is developed and validated, which shows good potential for geostationary satellites to swiftly detect active fires. Similarly, in [15], an early wildfire detection system was developed to monitor the wildfires in the Eastern Mediterranean using METEOSAT Second Generation (MSG) Spinning Enhanced Visible and Infrared Imager (SEVIRI), which provides coverage over Africa and Europe. GOES-R Active Fire product is based on WildFire Automated Biomass Burning Algorithm (WF_ABBA) proposed by [16]. It is a threshold-based method which preserves original spatial resolution and temporal resolution of GOES-R. The proposed GOES-R Active Fire product is evaluated in [17][18], the authors argue the active fire product is not adequately reliable, with false alarm rate around 60% to 80% for medium and low confidence fire pixels. How to swiftly detect active fire with limited false alarms remains a challenge in early fire detection. Deep learning models like Convlutional Neural Network and Recurrent Neural Network, as a state-of-the-art statistic tools, is widely used in classification problems of remote sensing images [19][20][21]. By leveraging low-level representations of the input data, deep learning models are capable of making robust classification in active fire detection. In [22], a deep learning algorithm based on convolutional neural network is adopted using GOES-16 images as the input to detect wildfires. The proposed method utilize spatial and spectral information to classify the center pixel of image patches. It shows optimal results in both detection time and accuracy for active fire detection. However, the study regions for the paper is limited and comprehensive detection time comparison between proposed method and other active fire product is needed. Also, the author utilize GOES-R images with the original $2km$ spatial resolution, the texture information within the patch is limited to make robust classification, as the size of the early stage active fire generate has smaller size than $4km^2$.

Because of the high temporal information of GOES-R data, it is easy to generate a time-series of images. However, research about early fire detection using temporal information of GOES-R images is limited. Therefore, it is desirable to evaluate deep learning-based models using GOES-R time series for early active fire detection in terms of both early detection time and false alarm rates. The objective of this research is to evaluate a deep learning model using GOES-R time series to achieve early detection of wildfires. In particular, a Recurrent Neural Network based model utilizing Gated Recurrent Units (GRU) [23] is proposed owing to its ability to model temporal information and high computational efficiency. The model utilizes the temporal information of low spatial resolution GOES-R time-series imagery and aims to achieve earlier detection time than that of VIIRS active

Preprints (www.preprints.org) | NOT PEER-REVIEWED | Posted: 18 July 2022 doi:10.20944/preprints202207.0265.v1

fire product from FIRMS and provide more precise location of early stage active fires than GOES-R active fire product.

2. Study Area and Data Description

Four large complex wildfires of California in 2020 are used as the training set and thirty eight different test areas are selected across North America and South America, as shown in Figure 1. For test regions in Tropical Climate Zone, the landcovers are mainly broafleaf forests on flat plains in the Amazon. For test areas in Subtropical Zone, landcovers are primarily Savanna located in mountainous terrain. Test sites in Temperate Zone generally have needleaf forests in mountains as their landcovers. Wildfires after 2018 are tested because of the availability of the GOES-R images. Due to the limitation in the coverage of the satellites, no study areas are outside North America and South America.

Table 1. Number of Test sites in Different Climate Zones.

Climate Zone	Number of Test sites
Tropical Zone	5
Subtropical Zone	12
Temperate Zone	21

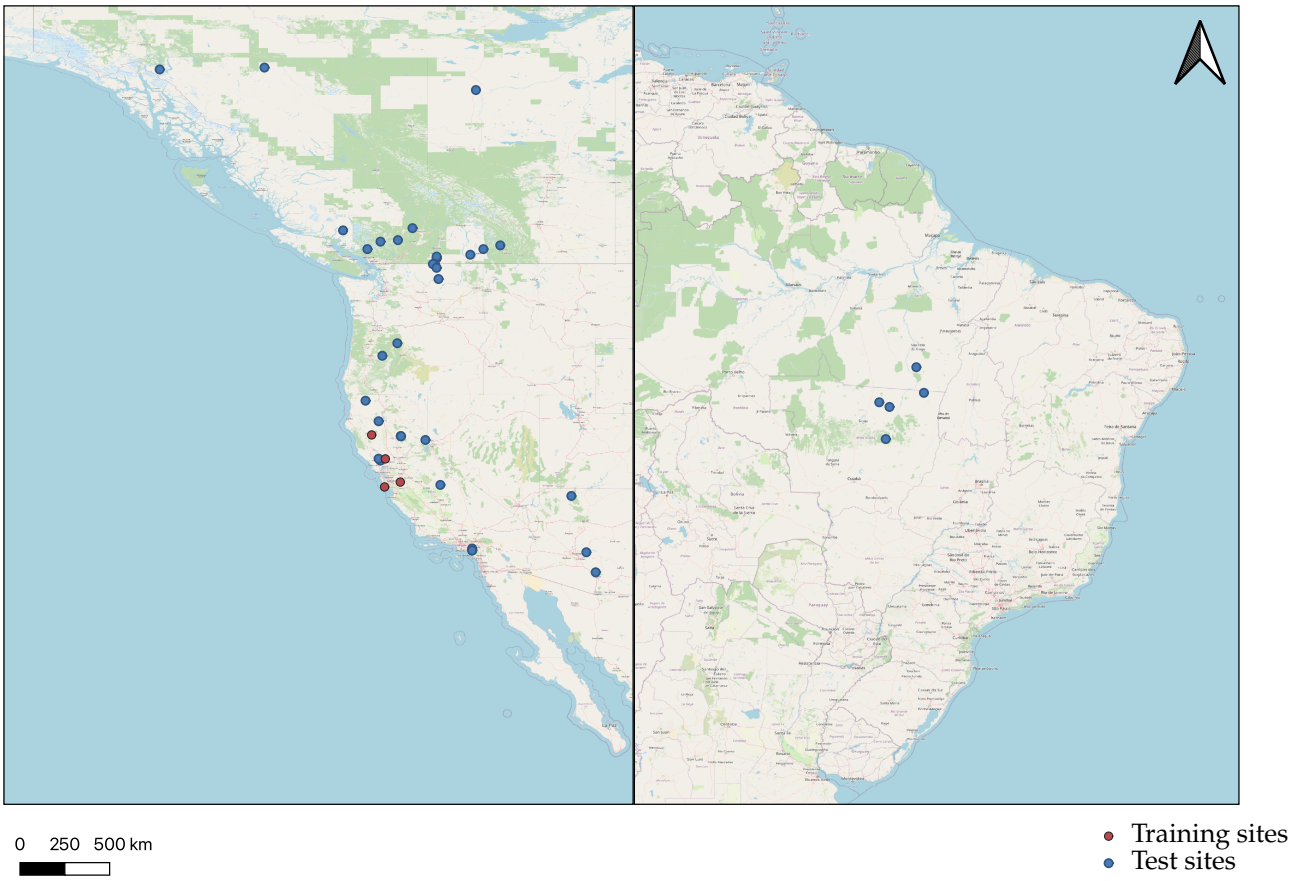

Figure 1. Study areas from North America and South America, all the wildfire regions are generated using QGIS and overlaid on Base Map Layer in Open Street Map

The Geostationary Operational Environmental Satellite-R series(GOES) are the geostationary weather satellites launched collaboratively by National Aeronautics and Space Administration(NASA) and National Oceanic and Atmospheric Administration(NOAA) of United States. GOES-R series consist of two satellites at two different operational longitude position. GOES-16 entered service from December 18th, 2017, and operates at east position

 doi:10.20944/preprints202207.0265.v1

of North America at longitude 75.2°West. It provides the full coverage of South America and East part of the North America. On the other hand, GOES-17 became operational from February 19th, 2019, and reached at west position at longitude of 137.2°West. Similarly, GOES-17 provides the full coverage of the west part of the North America, including British Columbia, Canada and Alaska, United States. Although the nominal spatial resolution for GOES-R Advance baseline Imager (ABI) images is 2 km, pixels grows larger when the latitude of the region increases because of the high azimuth angle. [18]

With the Advance baseline Imager on boarding as the primary instrument, GOES-R series satellites are able to capture optical images with four times spatial resolution than previous generations of GOES satellites [24]. Among all the spectral bands, Middle Infrared (MIR) band 7 at 3.80-4.00 μm wavelength is widely used in multiple different active fire products. The main reason is that the spectral radiance of burning biomass generally locates in Middle Infrared [25]. Also, Thermal Infrared (TIR) band 14 at 10.8-11.6 μm and band 15 at 11.8-12.8 μm wavelength can provide a good contrast between the burning biomass and non-burning areas. At the same time, TIR can be effective to distinguish clouds with active fire. Thus, it becomes the perfect candidate for cloud masking. As shown in Figure 2, points from the active fire areas and non-active fire areas are randomly sampled separately. The mean values of band 7, band 14 and band 15 are calculated for randomly sampled points in burning areas and non-burning areas. It can be observed that band 7 in MIR has significant high value in active fire areas while all three bands stay relatively the same for non-active fire areas.

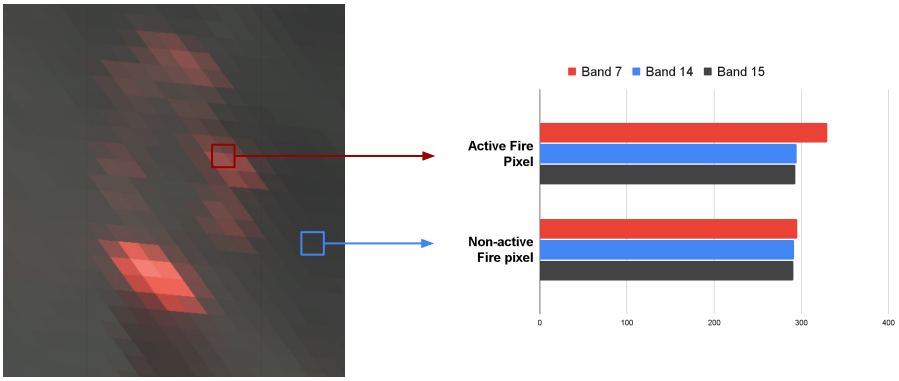

Figure 2. Inspections on the values of different bands for burning areas and non-burned areas. On the left hand side is the GOES-R ABI image captured at 6 PM on 2020-09-08, with composition R: Band 7, G: Band 14, B: Band 15. On the right hand side is the mean of three bands within burning areas and non-burning areas which are randomly sampled from the original image.

Due to the lack of ground truth data for the full progression of the active fire, Suomi-NPP VIIRS 375m Fire product serves as the training labels. VIIRS active fire product provides twice daily active fire mapping. Similar to GOES-R spectral bands, VIIRS also provides band I4 at 3.55-3.90 μm utilized to detect active fire and band I5 at 10.5-12.4 μm served as the main contrast band to I4. Moreover, VIIRS active fire product offers 375 spatial resolution with low error of commission and error of omission [9]. Considering GOES-R has a spatial resolution of 2 km, VIIRS active fire product is thus suitable to be used as the training labels.

Preprints (www.preprints.org) | NOT PEER-REVIEWED | Posted: 18 July 2022 doi:10.20944/preprints202207.0265.v1

3. Methodology

The overall methodology of GRU-based early fire detection using GOES-R data is shown in Figure 3. The main framework mainly consists of two parts, preprocessing for embedding generation and Deep GRU network for active fire detection.

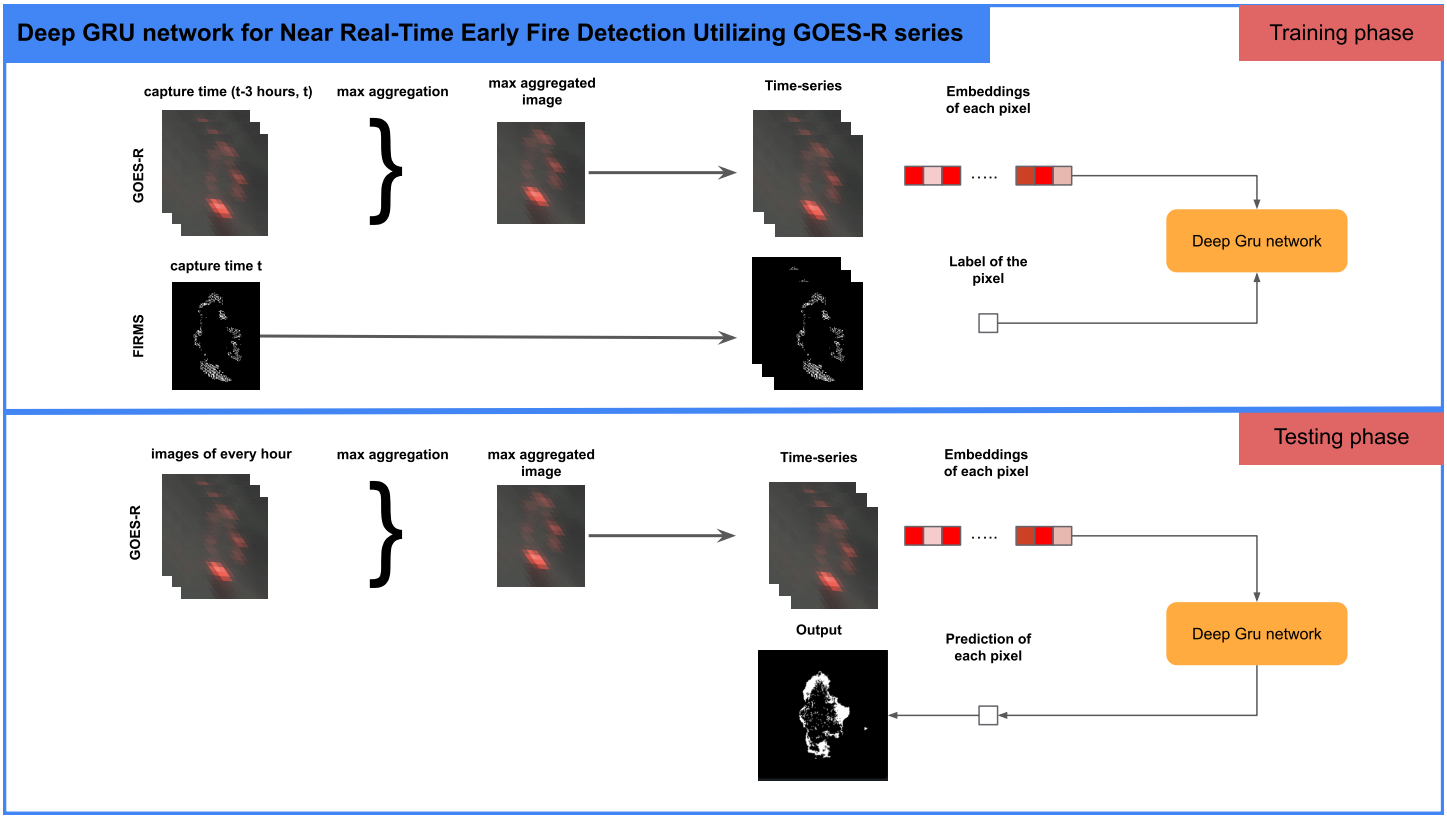

Figure 3. Deep GRU Network for Early Fire Detection

3.1. Dataset Generation and Preprocessing

The GOES-R dataset is pre-processed using Google Earth Engine [26]. As discussed in Section 2, MIR Band is sensitive to burning biomass on the ground, and TIR band is served as the a good contrast to the MIR band. Thus, the images(I_{active_fire}) used to generated the dataset are the normalized difference between MIR band iamges and TIR band images.

$$I_{active\_fire} = \frac{Band_7 - Band_{14}}{Band_7 + Band_{14}} \tag{1}$$

To provide an insight on the effect of the normalized difference I_{active_fire}, points from active fire and non-active areas are randomly sampled separately to generate the time-series over one day. As shown in Figure 4, the time series of band 7, band 14 and proposed normalized difference I_{active_fire} for burned area and unburned area clearly shows normalized difference can help better distinguish the active fire pixels from the background.

Furthermore, Band 15 with wavelength $\lambda_{15} = 11.8 - 12.8\ \mu$m is served as the cloud mask:

$$Cloud\_mask = Band_{15} > 280 \tag{2}$$

Even though GOES-R has high temporal resolution, it is difficult to find the matching image pair at the exact same timestamp. Because of the high dynamic of the cloud and smoke, several minutes difference can lead to a very different image. By applying max aggregation to all images within 3 hours before the capture time of VIIRS images, it can

Preprints (www.preprints.org) | NOT PEER-REVIEWED | Posted: 18 July 2022 doi:10.20944/preprints202207.0265.v1

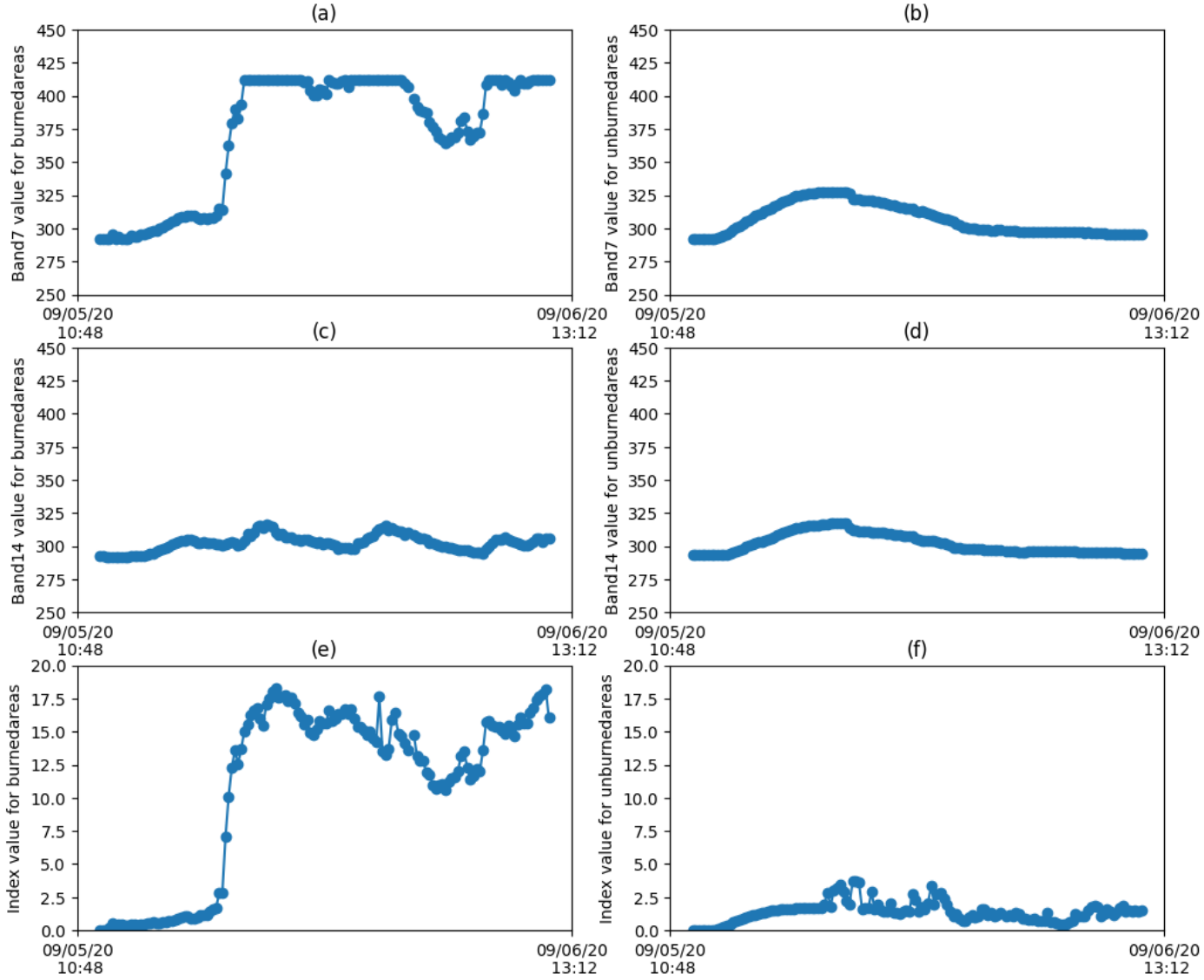

Figure 4. Inspections on time series of Band 7(a), Band 14(c), and Normalized difference value(e) of Burned area and time series of Band 7(b), Band 14(d), and Normalized difference value(f) of Unburned area. Study area: Creek Fire, California between 2020-09-05 12:00 to 2020-09-06 12:00

effectively reduce the interference of the cloud and smoke, so that the active fire pixels can match each other between two images. Hence, the aggregated images are served as the input data source.

However, the main challenge is the coarse resolution of GOES-R images. Considering the training label has 375 m spatial resolution, GOES-R images are bilinear resampled from 2 km spatial resolution to 375 spatial resolution. Due to the reason that the upsampled GOES-R images are still coarse in texture information, we propose pixel-level classification instead of object-level classification.

To better classify each pixel, it is necessary to encode spatial information into the embeddings of each pixel. To generate the embeddings of each pixel, two steps are involved. 1) The first step is to take an 11 by 11 image patch, and then flatten the image patch into a vector. We take patch size as 11 according to the number of pixels of the upsampled images within the distance between the center of two pixels of the original low-resolution images. This vector serves as the embedding for the center pixel in the patch. 2) The second

Preprints (www.preprints.org) | NOT PEER-REVIEWED | Posted: 18 July 2022 doi:10.20944/preprints202207.0265.v1

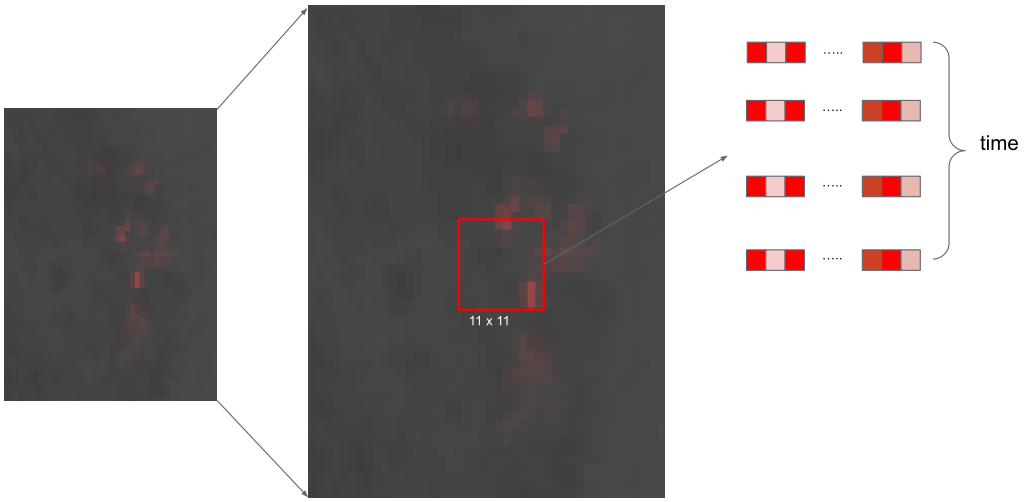

Figure 5. Preprocessing of the GOES-R imagery to generate time-series embeddings

step is to stack all the vectors for the same center pixel in different timestamps to form the time-series. The resulting time-series of the vectors are used as the input of the model.

As shown in the Figure 6, the time-series of the embeddings show the progression of the wildfire. For each row, it represents the flattened 11 by 11 image patch. The neighboring pixels above the center pixel locates in the columns of the left, while the neighboring pixels below the center pixel are in the right columns. And the center pixels locates at column 60. For each column, it represents the fluctuation of band values. When the wildfire progresses from top-right to bottom-left in given image patch, the highest value in its neighborhood flows from left to right in the embedding. And for each 11 pixels in the embedding map, it can be observed that bright spots shifted from right to left. Especially, when the highest value locates at the center pixel, the center pixel is more likely to be classified as the fire pixel. The time-series model is possible to leverage the fluctuation of values of center pixel and its neighboring pixels at all previous timestamps to classify the center pixel.

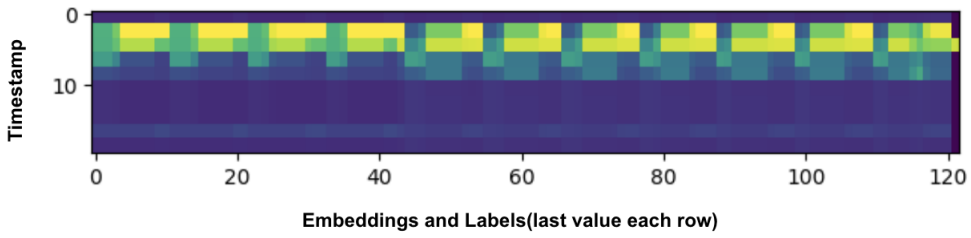

Figure 6. Time-series of embedding, x-axis represents the embedded vector for each pixel and its neighborhood pixels and its corresponding label at the last column, y-axis represents the timestamps. The figure shows the embedding for the first 20 timestamps for one image patch.

3.2. Deep GRU network

3.2.1. Gated Recurrent Unit

To process the time-series of the embedding, we propose to use Recurrent neural network. As shown in Figure 7, at timestamp t, the basic architecture of recurrent neural

Preprints (www.preprints.org) | NOT PEER-REVIEWED | Posted: 18 July 2022 doi:10.20944/preprints202207.0265.v1

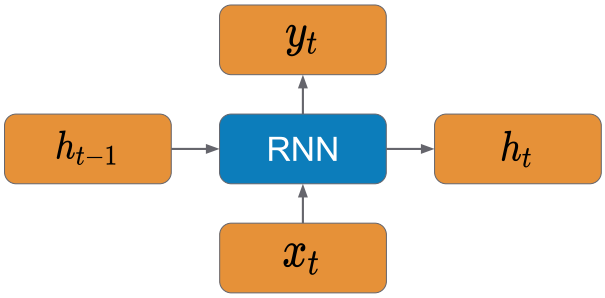

Figure 7. Basic Architecture of Recurrent neural network

network consists of input x_t, output y_t and hidden state h_t. Like feed forward network, input at each timestamp is fed into the network with weights and biases in the hidden neuron. Recurrent Neural network also utilizes the hidden state from previous timestamp and combine it with the input to generate the output. Owing to this sequential architecture, recurrent neural network has become the standard to process time-series data, because the output of each timestamp is high correlated with the hidden states of the previous timestamps.

Among all the RNN variants, Gated Recurrent Unit [23] and Long Short Term Memory (LSTM) [27] are known to be the most well-known one which solves the problem within classical recurrent neural network like gradient vanish and capable to keep long term memory. As shown in Fig 8, inside GRU, there are two major components, reset gate and update gate. Reset gate defines the amount of information from previous hidden state to be forgot. The output of reset gate r_t and update gate can be calculated in Equation 3 and Equation4, in which, $\mathbf{W}_r$ and $\mathbf{W}_z$ are weight matrix for the input, $\mathbf{U}_r$ and $\mathbf{U}_z$ are weight matrix for hidden state.

$$r_t = \sigma([\mathbf{W}_r\mathbf{x}]_t + [\mathbf{U}_r\mathbf{h}_{<t-1>}]_t) \tag{3}$$

$$z_t = \sigma([\mathbf{W}_z\mathbf{x}]_t + [\mathbf{U}_z\mathbf{h}_{<t-1>}]_t) \tag{4}$$

The output of GRU can be calculated as Equations 5 and 6. ϕ is the activation function of the GRU, $\mathbf{W}$ and $\mathbf{U}$ are weights to calculate the intermediate result. Output of Reset Gate r_t is multiplied element-wise with the hidden state of the previous timestamp. When r_t is close to 0, that means previous hidden state is dropped in calculating the intermediate output. Then the output of Update Gate z_t defines the weights of the previous output and the intermediate output in the output of the GRU at current timestamp.

$$\tilde{h}_t = \phi([\mathbf{W}\mathbf{x}]_t + [\mathbf{U}(\mathbf{r} \odot \mathbf{h}_{t-1})]_t) \tag{5}$$

$$h_t = z_t h_{t-1} + (1 - z_t)\tilde{h}_t \tag{6}$$

LSTM is a generalization of GRU, but it also has two extra gates, output gate and forget gates. Output gate defines the percentage of output to be used in the hidden state in the next timestamp, but the output of GRU is equivalent to the new hidden state. Forget gate which defines whether or not to erase the previous hidden state, but in GRU, it is calculated directly by using 1 minus the output of update gate. In this case, GRU has around half of the parameters compared to LSTM because of less gates involved in the calculation. Compared to LSTM, GRU is computationally cheaper, and can provide similar performance as LSTM [28]. Because early fire detection is a time-critical application, we choose GRU as the basic unit of the network to reduce the computation time in training and prediction phase.

Preprints (www.preprints.org) | NOT PEER-REVIEWED | Posted: 18 July 2022 doi:10.20944/preprints202207.0265.v1

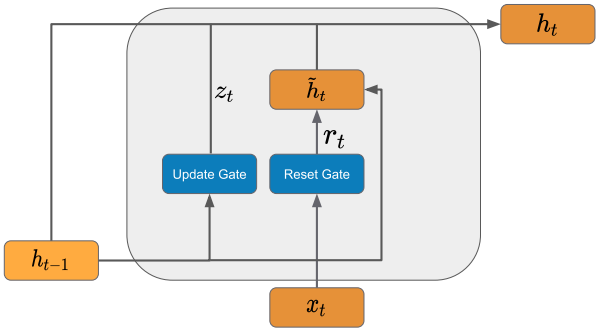

Figure 8. Architecture of Gated Recurrent Unit

3.2.2. Deep GRU network

In this section, we propose the Deep GRU Network to best utilize the time-series information for all the images. As shown in Figure 9, this network is implemented as a 6 layers architecture. We run a set of models using different hyperparameters, and the parameters shown in Table 2 give the best result. The network consists of 5 layers GRU network with many-to-many architecture and one level of Dense network to generate the output.

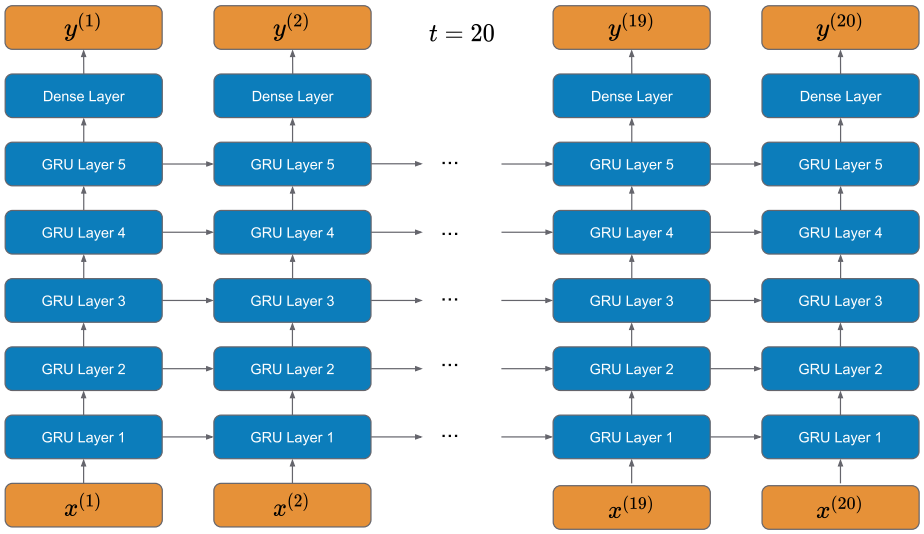

Figure 9. Deep GRU network architecture

As shown in the Table 2, the network takes a sequence of 20 vectors of pixels as the input for 20 different timestamps. And for each vector, it corresponds to one image patch from the image with one center pixel and all its neighboring pixels. The deep GRU network proposed consists of 5 GRU layer with 256 hidden states. At the output layer, there is one single dense layer applied across all the timestamps with sigmoid activation function, which generate the classification for the center pixel.

3.2.3. Loss Function

The training label is in one-hot format and there are two classes fire/non-fire for each center pixel. Since the number of non-fire pixels is much more than the number of fire

Preprints (www.preprints.org) | NOT PEER-REVIEWED | Posted: 18 July 2022 doi:10.20944/preprints202207.0265.v1

Table 2. Detail Structure of Deep GRU Network

Layers	Layer type	Input size	Output size
Input Layer	Input Layer	N/A	(20, 121)
Layer #1	Dense Layer	(20, 121)	(20, 512)
Layer #2	GRU Layer	(20, 512)	(20, 512)
Layer #3	GRU Layer	(20, 512)	(20, 512)
Layer #4	GRU Layer	(20, 512)	(20, 512)
Layer #5	GRU Layer	(20, 512)	(20, 512)
Layer #6	GRU Layer	(20, 512)	(20, 512)
Output Layer	Dense Layer	(20, 512)	(20, 2)

pixels, Focal loss [29] is used as the loss function. Shown as Equation 7, Focal loss is widely used in classification of the highly unbalanced dataset.

$$FocalLoss = -\alpha(1-p_t)^{\gamma}log(p_t) \tag{7}$$

$$p_t = \begin{cases} p, \text{ fire pixel} \\ 1-p, \text{ non-fire pixel} \end{cases} \tag{8}$$

In which, p_t in Equation 8 is the probability of pixels being classified as fire or non-fire pixels. γ is the focusing parameter used in the modulating factor $(1-p_t)^{\gamma}$, the modulating factor decreases to nearly zero when classifying samples from one class which dominates the dataset. This behavior down-weights the well-classified samples, and in this scenarios is the non-fire pixels. While for fire pixels, since the probabilities are low, the modulating factor is close to 1, and it does not change the loss. α is the weighting factor, and it gives different weights to different factors. Modulating factor and weighting factor both try to reduce the loss value caused by accumulating errors from mis-classification of easy samples.

3.3. Testing Stage

3.3.1. Preprocessing and Inferrencing

To achieve near real-time requirement, the input data for inference is slightly modified to achieve higher time requirements. Alternatively, max-aggregated GOES-R images for each hour are used in inference. Although, the interference of smoke and cloud can become higher because less images are aggregated together. To reduce the mis-classification caused by smoke and clouds, a threshold is applied to each pixel. Based on our experiment, the best performance for mid latitude and high latitude region is obtained when the threshold equals to 4. In terms of the low latitude regions like Amazon forest in Brazil, the threshold is set to 1.

3.4. Setup

All the satellite images are collected from Google Earth Engine [26] and the deep learning model is developed using Tensorflow [30]. The training dataset is composed of 4 large-scale wildfires from California in 2020. The test dataset consists of max-aggregated images from 36 study areas across North America and South America as shown in Figure 1. For the detection time evaluation, we only detect the earliest time when there are fire pixels in the output images. While for accuracy assessment, the error of commission and error of omission on the burned area for three study areas in North America will be discussed in Section 4. After preprocessing, in total 60000 samples which consists of time-series of vectors of pixels are used in training. In terms of the processing platform, we trained our network using NVIDIA Tesla K80 GPU from Google Colab with minibatch size of 128. By applying the Adam optimizer with learning rate $l_r = 0.001$, the network coverage in 10 epochs. The training loss curve is shown in Figure 10.

Preprints (www.preprints.org) | NOT PEER-REVIEWED | Posted: 18 July 2022 doi:10.20944/preprints202207.0265.v1

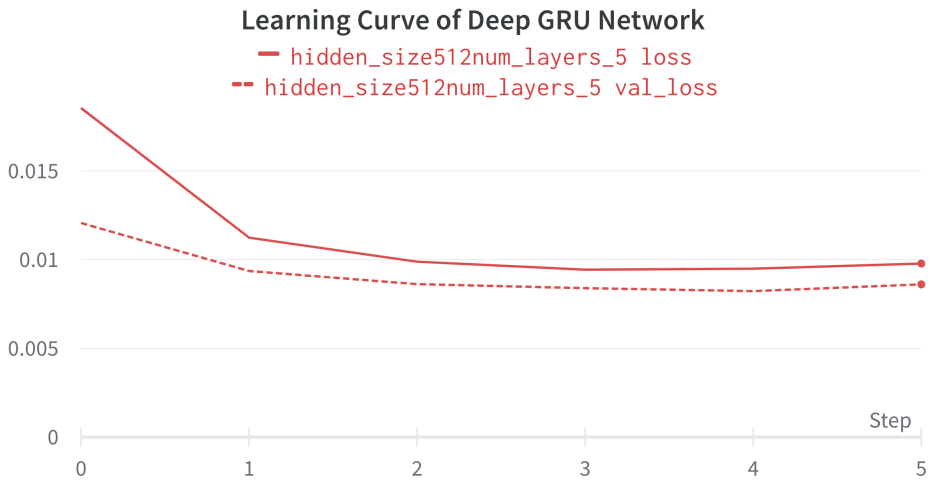

Figure 10. Learning Curve of proposed Deep GRU model with training loss and validation loss.

3.5. Accuracy Assessment

The assessment of the network is based on two factors: 1)the earliest detection time, 2) accuracy assessment on the burned areas.

For the earliest detection, the proposed method is compared with FIRMS VIIRS fire product, which provides active fire detection twice a day. The earliest detection time of the proposed method is based on earliest time when fire pixels appear in the output images.

For the accuracy assessment, Difference Normalized Burned Ratio(dNBR) of Sentinel-2 image is served as the reference for the accuracy assessment. The dNBR is calculate based on the difference on Normalized Burned Ratio between post-fire image and the pre-fire image. To evaluate the accuracy for early stage wildfire, the post-fire image is the earliest Sentinel-2 image after the wildfire. And the pre-fire image is using averaged Sentinel-2 image for the past 3 months before the wildfire. Finally, the burned area can be obtained by thresholding the Difference Normalized Burned Ratio. To follow the same spatial resolution of the output of the proposed method, the Sentinel-2 images are downsampled to 375 m spatial resolution. In this experiment, we use threshold $TH = 0.1$.

$$dNBR = NBR_{pre\_fire} - NBR_{post\_fire} \tag{9}$$

$$NBR = \frac{Band_{NIR} - Band_{SWIR}}{Band_{NIR} + Band_{SWIR}} \tag{10}$$

Besides the proposed method, FIRMS VIIRS fire product and GOES-R fire product are also tested on the same study area for comparison. GOES-R active fire product serves as the baseline of the accuracy assessment as it is based on the same data source. Due to the reason that these remote sensing images all have lower spatial resolution than Sentinel-2 images, dNBR of Sentinel-2 images are used as the ground truth. There are four different evaluation metrics. Following the evaluation done by [6], independent error of commission and independent error of omission are evaluated for direct burned area mapping. Error of Commission is characterized as the false alarm, where the image patch from Sentinel-2 corresponding to the fire pixel in low resolution images does not contain any burned areas. In same sense, Error of Omission is defined that where the image patches from Sentinel-2 contain burned area but low resolution images fail to detect. Furthermore, classical evaluation metrics for image segmentation like F1 score and Intersection over Union(IoU) are provided. The equation for F1 score and IoU score are shown in Equation 11,12. In the

 doi:10.20944/preprints202207.0265.v1

euqation, TP means True Positive detection, FP is False Positive detection and FN is False Negative detection.

$$\text{F1 Score} = \frac{TP}{TP + \frac{1}{2}(FP + FN)} \tag{11}$$

$$\text{IoU Score} = \frac{TP}{TP + FP + FN} \tag{12}$$

4. Results and Discussion

4.1. Earliest detection of active fires

In this section, the detection time of proposed method is compared with the FIRMS VIIRS active fire product. Because of the nature of the proposed method that the max-aggregated image over each hour is used as the input, the detection time of the proposed method is also provided as a period on the imaged used as the input.

As shown in Table 3, the proposed method utilizing GOES-R time-series can detect 24 out of 38 wildfires earlier than VIIRS and 6 out of 38 wildfires similar to VIIRS, and 8 out of 38 wildfires later than VIIRS. In total, 78.95% of the wildfire can be detected earlier with the proposed method than VIIRS. Regionally, most of the wildfires at all locations show earlier or similar detections. Especially, the early detection time show premium result in United States and Brazil. For the earlier detections, proposed methods can detect fire spots within the half-day gap between 2 VIIRS images. For the wildfires with similar detection time, there are two different scenarios. The first one is when the emerging of the wildfire is covered by the heavy cloud. And at the detection time when the fire spot is visible from both of the instruments, it has been large enough to be detected by both of the methods. The second scenario is when the capture time of VIIRS coincidence with GOES-R capture time, and the fire radiance power of the wildfire is high enough for coarse resolution GOES-R to detect.

However, there are still some regions having later detection time than the VIIRS detection. Regionally, 6 out of 8 late wildfire detection are located in Canada, and 2 of 8 are located in United States. The result indicates late detections are often in high latitude regions like Canada. It is because of the difference in orbits of Suomi-NPP and GOES-R. GOES-R is geostationary satellites with orbit locates at the equator. By its nature, there is distortion for contours in high latitude region due to the slant viewing angle. In contrast Suomi-NPP is an polar-orbiting satellite, and there is no distortion in high latitude region as the satellite directly pass above those regions. Hence, the footprint of GOES-R in high latitude regions is larger then footprint of low and mid-latitude regions. It leads the spatial resolution of the GOES-R images decreases significantly. As a result, the early stages of the wildfires in those regions are difficult to detect. For other late detections in United States, the main reason is the tested fire has low fire radiance power in early stages. For example, the emerging of the wildfire coincides with the capture time of VIIRS, and the active fire is in small scale. In this case, the advantage of high spatial resolution of VIIRS would help detect the fire with low fire radiance power(FRP). It is difficult for Deep GRU network to extract the fire pixels out of the GOES-R image, since the area covered by one GOES-R pixel equals nearly 28 times larger than the areas covered by one VIIRS pixel.

4.2. Accuracy assessment

For this section, the accuracy of the proposed method is assessed by comparing the burned area with other available active fire products. Since the proposed method detects the active fire instead of burned area, in this experiment, the burned area is obtained by accumulating the active fire pixels before the capture time of the Sentinel-2 image which serves as the ground truth.

The creek fire, currently the fourth largest fire in California's history, starts from September 4th, 2020. This tremendous wildfire caused 153,738 hectares of land burned which mostly belongs to Sierra National Forest. Noticeably, from September 4th, 2020 to

Preprints (www.preprints.org) | NOT PEER-REVIEWED | Posted: 18 July 2022 doi:10.20944/preprints202207.0265.v1

Table 3. Comparison over all study areas for FIRMS detection time and Deep GRU network detection time, '+1' means the detection of the active fire happens on the next day of the start date. The name of the wildfire are either named after fire names from The Department of Forestry and Fire Protection of California, fire numbers from British Columbia Wildfire Service, fire numbers from 2020 Major Amazon Fires Tracker, developed by InfoAmazonia, and the location of the wildfire where it happens.

Location	Fires	Start date	Location	FIRMS time	GOES time	Result
California, US	Creek fire	2020-09-05	(-119.30, 37.20)	09:06	06:00-07:00	Earlier
	Blue Ridge Fire	2020-10-26	(-117.68, 33.88)	09:06	06:00-07:00	Earlier
	Silverado Fire	2020-10-26	(-117.66, 33.74)	07:54	06:00-06:59	Earlier
	Bond Fire	2020-12-02	(-117.67, 33.74)	09:12	08:00-09:00	Earlier
	Glass Fire	2020-09-27	(-122.50, 38.57)	21:06	11:00-12:00	Earlier
	North Complex Fire	2020-08-14	(-120.12, 39.69)	05:47 +1 day	20:00-21:00	Earlier
	Camp Fire	2018-11-08	(-121.43, 39.81)	18:14	15:00-16:00	Earlier
	Tubbs Fire	2017-10-08	(-122.63, 38.61)	06:32	05:00-06:00	Earlier
	Carr Fire	2018-07-23	(-122.62, 40.65)	21:08	21:00-22:00	Similar
	Dixie Fire	2021-07-14	(-121.42, 39.81)	20:30	05:00-06:00	Earlier
British Columbia, Canada	N21257	2020-08-18	(-116.10, 50.09)	20:18	18:00-19:00	Earlier
	N51250	2020-08-17	(-117.01, 49.85)	20:42	22:00-23:00	Later
	N51287	2020-08-18	(-119.54, 49.36)	22:00	22:00-23:00	Similar
	V30067	2020-04-15	(-123.22, 49.88)	11:01	00:00-01:00	Earlier
	R90376	2019-05-27	(-128.70, 59.55)	22:26	22:00-23:00	Similar
	K51244	2019-08-05	(-119.50, 49.42)	20:30	19:00-20:00	Earlier
	R90881	2019-08-03	(-134.35, 59.43)	22:52	22:00-23:00	Similar
	K50271	2019-05-13	(-119.66, 49.04)	10:06	20:00-21:00	Earlier
	K51089	2019-07-26	(-119.70, 49.06)	21:58	01:00-02:00 +1 day	Later
	N71114	2020-08-19	(-117.70, 49.58)	08:36	01:00-02::00	Earlier
	V31179	2020-08-18	(-122.50, 50.20)	08:54	18:00-19:00	Later
	V51227	2020-08-17	(-124.53, 50.84)	20:45	20:00-21:00	Similar
	Lytton Fire	2021-06-29	(-121.57, 50.28)	10:30	22:00-23:00	Later
	Sparks Lake Fire	2021-06-28	(-120.79, 50.92)	21:54	00:00-01:00 +1 day	Later
Alberta, Canada	Chuckegg Creek Fire	2019-05-17	(-117.42, 58.38)	08:59	21:00-22:00	Later
Arizona State, US	The bush fire	2020-06-13	(-111.56, 33.63)	09:18 +1 day	20;00-20:59	Earlier
	The magnum fire	2020-06-08	(-112.34,36.61)	09:20 +1 day	22:00-23:00	Earlier
	Bighorn fire	2020-06-06	(-111.03,32.53)	09:18	11:00-12:00	Later
Oregon State, US	Holiday farm fire	2020-09-07	(-122.45, 44.15)	09:00	05:00-06:00	Earlier
	Slater fire	2020-09-07	(-123.38, 41.77)	20:24	15:00-16:00	Earlier
	Beachie creek fire	2020-08-17	(-121.62,44.77)	09:12	10:00-11:00	Later
Amazon, Brazil	brazil_fire_1214	2020-09-05	(-51.61, -9.894)	16:06	14:00-15:00	Earlier
	brazil_fire_668	2020-09-01	(-54.49, -10.52)	04:42	00:00-01:00	Earlier
	brazil_fire_675	2020-08-31	(-53.83, -10.80)	05:00	00:00-01:00	Earlier
	brazil_fire_1341	2020-09-02	(-54.07,-12.87)	04:06	00:00-01:00	Earlier
	brazil_fire_728	2020-09-02	(-52.10, -8.24)	17:00	14:00-15:00	Earlier
Washiton State, US	Palmer fire	2020-08-18	(-119.56, 48.83)	22:00	22:00-23:00	Similar
	Cold spring fire	2020-09-07	(-119.49, 48.29)	11:00	06:00-07:00	Earlier

Preprints (www.preprints.org) | NOT PEER-REVIEWED | Posted: 18 July 2022 doi:10.20944/preprints202207.0265.v1

September 9th, 2020, this wildfire expands between 20,000 acres to 50,000 acres each day. This speed of expansion further proves the early detection and rapid progression mapping of wildfire is time-critical.

As shown in Fig 11, burned area progression mapping generated from VIIRS 375m active fire product and proposed method are compared each day after the emerging of the wildfire. For evaluation purpose, the earliest possible Sentinel-2 image can be obtained at 17:30 GMT, 2020-09-08. Each VIIRS burned area mapping is generated by accumulating the available day and night capture at around 08:30 GMT and 20:30 GMT and overlaying on burned areas of previous days. As for the proposed Deep GRU network, the outputs at each hour are accumulated and overlaid on all previous output binary maps. For the baseline, active fire points of GOES-R active fire product before the capture time of Sentinel-2 are accumulated for the same area of interest.

By visually comparing the result, we could find that burned area images from VIIRS are sparse, the reason is partly because of lack of captures for some of the active fire points and partly about the error introduced when transferring VIIRS raster to active fire points when developing the active fire product. Compared to VIIRS images, the proposed method generated overestimated burned areas because of the low spatial resolution. The baseline for accuracy assessment, GOES-R active fire product, can bared cover the correct location of the burned area and that commits both high error of commission and error of omission. Quantitatively, proposed method provides the lowest error of omission and comparable error of commission compared with FIRMS for the Creek Fire as shown in Table 4. At the same time, the proposed method outperforms the baseline in F1 Score and mIoU and shows comparable numbers to VIIRS, which serves as the training label in the training phase. That indicates the proposed method could show preciser location than GOES-R Active Fire product in this study region.

Table 4. Accuracy Evaluation on burned area mappings using VIIRS active fire product, GOES-R active fire product, output of proposed Deep-GRU network based on GOES-R images, output of Support Vector Machine(SVM) and Random Forest using GOES-R images.

Study Area	VIIRS 375m Active Fire product	GOES-R Active Fire product	Deep GRU output	SVM	Random Forest
Error of Omission					
Creek Fire	14.71%	13.83%	0.81%	0.23%	0.13%
Camp Fire	49.51%	61.36%	0.40%	0.13%	0.16%
Doctor Creek Fire	16.93%	0%	0%	0.48%	0.48%
Error of Comission					
Creek Fire	15.96%	60.02%	44.41%	72.92%	73.78%
Camp Fire	18.34%	78.97%	53.57%	63.37%	62.52%
Doctor Creek Fire	43.32%	96.76%	89.86%	92.28%	92.32%
F1 Score					
Creek Fire	0.8466	0.5462	0.7125	0.4259	0.4203
Camp Fire	0.6239	0.2724	0.6333	0.5360	0.5450
Doctor Creek Fire	0.6738	0.0629	0.1841	0.1432	0.1425
Intersection Over Union(IoU)					
Creek Fire	0.7340	0.3757	0.5534	0.2706	0.2661
Camp Fire	0.4534	0.1576	0.4634	0.3662	0.3746
Doctor Creek Fire	0.5081	0.0324	0.1014	0.0771	0.0767

The Camp Fire is the deadliest and most destructive wildfire in California's history. With 62 052.8 hectares of land being burned, this wildfire happened in Northern California's Butte County, and lasted nearly two weeks from 2018-11-08 to 2018-11-25.

From Figure 12, it can be observed that the wildfire progresses extremely fast in the first day. The earliest capture of the Sentinel-2 images is on 2020-11-11. Compared with Sentinel-

Preprints (www.preprints.org) | NOT PEER-REVIEWED | Posted: 18 July 2022 doi:10.20944/preprints202207.0265.v1

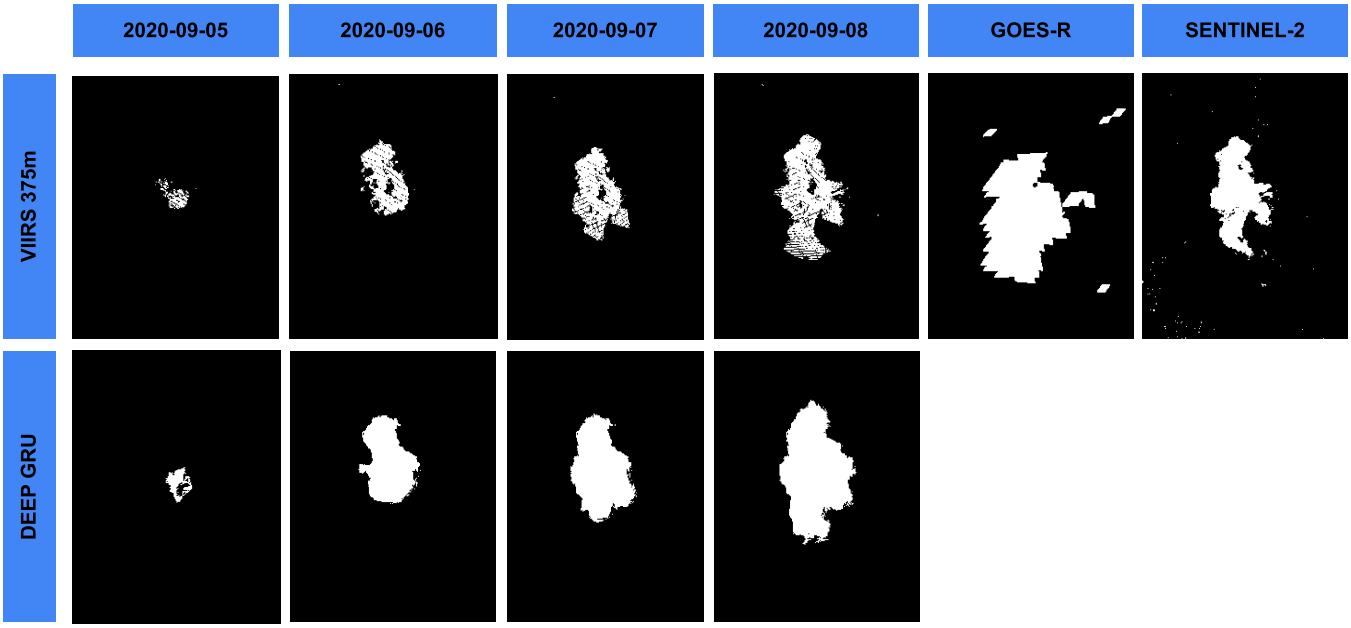

Figure 11. Burned area progression mapping of VIIRS 375m active fire product and proposed method for 2020-09-05 to 2020-09-08 until Sentinel-2 image is available. Accumulated image from GOES-R active fire product from 2020-09-05 to 2020-09-08 is served as the baseline.

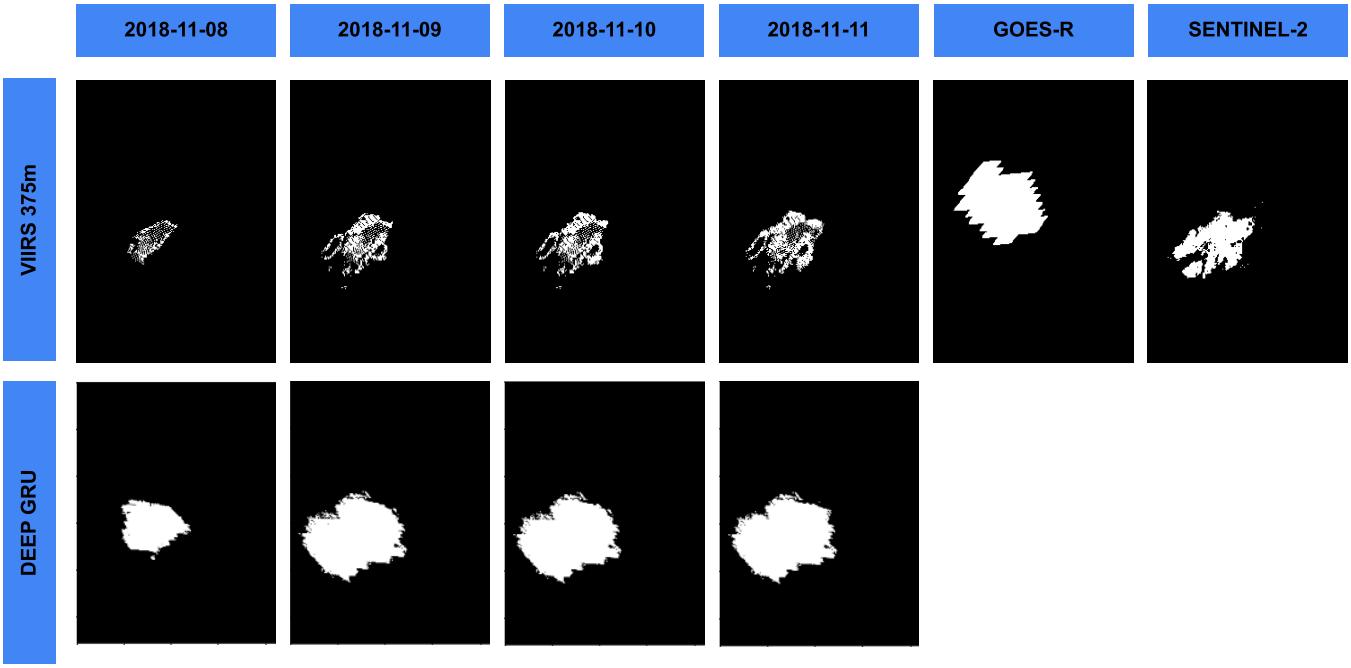

Figure 12. Burned area progression mapping of VIIRS 375m active fire product and proposed method for 2018-11-08 to 2020-11-11 until Sentinel-2 image is available. Accumulated image from GOES-R active fire product from 2018-11-08 to 2020-11-11 is served as the baseline.

Preprints (www.preprints.org) | NOT PEER-REVIEWED | Posted: 18 July 2022 doi:10.20944/preprints202207.0265.v1

2 dNBR image, VIIRS active points have some underestimations on the burned areas, which leads to high error of omission as shown in Table 4. In contrary, proposed method also overestimates the burned area, which caused relatively high error of commission compared to VIIRS. However, for both F1 score and mIoU, proposed method outperforms VIIRS 375m active fire product and GOES-R active fire product. The baseline GOES-R active fire product conducts both high error of commission error and error of omission, which makes both the F1 score and mIoU much lower than both of the methods.

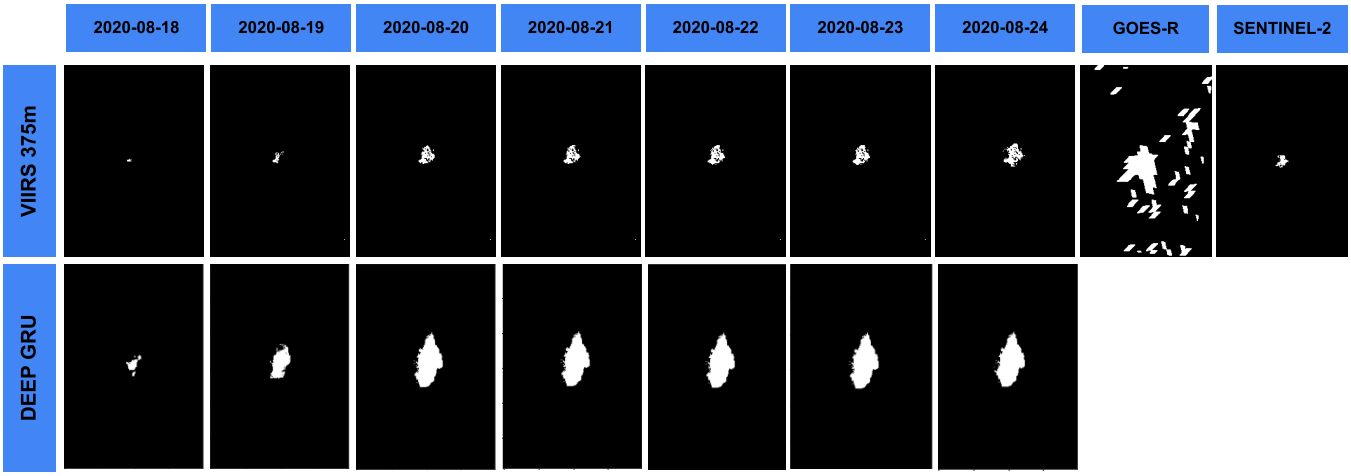

Figure 13. Burned area progression mapping of VIIRS 375m active fire product and proposed method for 2020-08-18 to 2020-08-24 until Sentinel-2 image is available.

The Doctor Creek Fire, started from September 19, locates at 25 kiolometers southwest of Canal Flats, British Columnbia, Canada. The size of this wildfire is 7,645 hectares, which is the largest wildfire of British Columbia for the whole 2020.

In Figure 13, the results are evaluated using the dNBR of Sentinel-2 images captured on 2020-08-24. Different from those two California wildfires evaluated previously, Doctor Creek fire has much smaller burned area and it locates at high latitude region. In this case, proposed method and GOES-R active fire product both have extremely high error of commission compared to VIIRS. The reason is also because of the distortion at high latitude regions as discussed in Section 4.1. Compared with the baseline GOES-R Active Fire product, false alarms of GOES-R active fire product are significantly higher than proposed method, and create pepper and salt noise in the image. Thus, the error of commission is higher than the proposed method. For the error of omission, proposed method has lower score because of the sparsity of the VIIRS active fire points. Both proposed method and GOES-R Active Fire product have 0 as the error of omission. This is because the overestimation of the burned area covers all the regions of the ground truth. Finally, the proposed method has higher F1 score and mIoU than GOES-R active fire points but lower than VIIRS 375m active fire product because of the distortion effect in high latitude district.

For comparison study, two classical machine learning algorithms Support Vector Machine(SVM) and Random Forest(RF) are trained using the same training dataset and tested over three test regions. From the Table 4, both SVM and RF shows better F1 score and IoU score compared to GOES-R Active Fire product. But the proposed Deep-GRU Network provides better performance than both of the machine learning models.

For the initial state of the wildfire, the proposed method could compare with the GOES-R active fire product since this is the only data available. As shown in Figure 14, for following study areas, the proposed method can detect the wildfire at about the same time as GOES-R active fire product. But owing to the proposed method actually upsampled the GOES-R ABI images to 375 spatial resolution, the proposed method can indicate smaller regions at the early stage of the wildfire. Although for Camp fire the effect is less significant, we argue that the emerging stage of this wildfire is not exactly captured because of the interference of cloud and smoke. And by the time the fire is detected, the size of the wildfire

 doi:10.20944/preprints202207.0265.v1

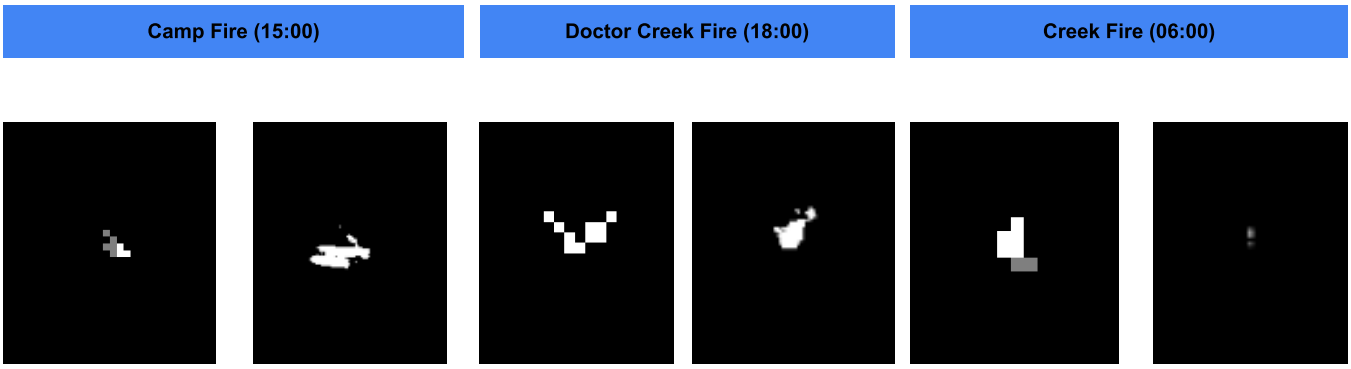

Figure 14. Emerging stage of the wildfire at three study areas and its capture time.

has been in large scale. Overall, the proposed method helps to identify the burning biomass in a smaller scale at the initial stage of the wildfire.

In conclusion, for burned area mapping, the proposed Deep GRU network utilizing GOES-R images can accurately monitoring the wildfire in mid-latitude regions like California. However, due to the strong distortion effect in high latitude district, the proposed method can have better accuracy than the baseline active fire product, but still not optimal to monitor the exact location of the burned areas.

5. Conclusions

In this research, we proposed Deep GRU network to detect active fires from GOES-R ABI images in the early stage of the wildfire. Based on the experiment on the study area, the proposed network can detect majorities of the wildfire earlier than VIIRS Active Fire product. At the same time, the proposed network can identify burned areas more accurately than GOES-R Active Fire product in the early stage, and significantly reduced the false alarm. By applying resampling and using 375 m spatial resolution VIIRS active fire points as training label, the output of the network also provide descent burned area mapping in mid-latitude region. The major contribution of this paper can be summaerized as follows:

- The proposed network leverage GOES-R time-series and is possible to detect majorities of the wildfire in study areas earlier than the wildly used VIIRS Active Fire Product in NASA's Fire Information for Resource Management System. The study areas spread across low-latitude regions mid-latitude regions and high-latitude regions. It shows good generalizability in detecting wildfires in the early stage.
- The proposed method provides good indication of areas affected by the wildfires in the early stage for low-resolution and mid-resolution regions compared to GOES-R Active Fire product. Especially, it significantly reduced the false alarms of GOES-R Active Fire product. For high-latitude regions such as Doctor Creek Fire in British Columbia, the detection shows high error of commission because of the distortion caused by the terminologies of geostationary satellites. Also, for the first detection of the active fire, the proposed method also shows more accurate location of the wildfire compared to GOES-R Active Fire product, while VIIRS active fire product is not available at that time.

Author Contributions: Conceptualization, methodology, implementation, validation, formal analysis, investigation, original draft preparation, Y.Z.; Conceptualization, resources, writing—review and editing, supervision, project administration, funding acquisition, Y.B. All authors have read and agreed to the published version of the manuscript.

Funding: The research is part of the project 'Sentinel4Wildfire' funded by Formas, the Swedish research council for sustainable development and the project 'EO-AI4Global Change' funded by Digital Futures.

Institutional Review Board Statement: Not applicable.

Informed Consent Statement: Not applicable.

Data Availability Statement: The datasets used in this study are available from on request from the authors.

Acknowledgments: In this section you can acknowledge any support given which is not covered by the author contribution or funding sections. This may include administrative and technical support, or donations in kind (e.g., materials used for experiments).

Conflicts of Interest: The authors declare no conflict of interest. The funders had no role in the design of the study; in the collection, analyses, or interpretation of data; in the writing of the manuscript, or in the decision to publish the results.

Sample Availability: Samples of the code are available from the authors.

Abbreviations

The following abbreviations are used in this manuscript:

EO	Earth Observation
DL	Deep Learning
GRU	Gated Recurrent Neural Network
LSTM	Long Short-Term Memory
GOES-R	Geostationary Operational Environmental Satellites R Series
SLSTR	Sea and Land Surface Temperature Radiometer
VIIRS	Visible Infrared Imaging Radiometer Suite
MODIS	Moderate Resolution Imaging Spectroradiometer

References

1. Canadell, J.G.; Monteiro, P.M.; Costa, M.H.; Da Cunha, L.C.; Cox, P.M.; Alexey, V.; Henson, S.; Ishii, M.; Jaccard, S.; Koven, C.; et al. Global carbon and other biogeochemical cycles and feedbacks, 2021.
2. Pradhan, B.; Suliman, M.; Awang, M.A.B. Forest fire susceptibility and risk mapping using remote sensing and geographical information systems (GIS). *Disaster Prevention and Management* **2007**, *16*, 344–352.
3. Hu, X.; Ban, Y.; Nascetti, A. Sentinel-2 MSI data for active fire detection in major fire-prone biomes: A multi-criteria approach. *Int. J. Appl. Earth Obs. Geoinformation* **2021**, *101*, 102347.
4. Schroeder, W.; Oliva, P.; Giglio, L.; Quayle, B.; Lorenz, E.; Morelli, F. Active fire detection using Landsat-8/OLI data. *Remote Sensing of Environment* **2016**, *185*, 210–220.
5. Kumar, S.S.; Roy, D.P. Global operational land imager Landsat-8 reflectance-based active fire detection algorithm. *International Journal of Digital Earth* **2018**, *11*, 154 – 178.
6. Schroeder, W.; Oliva, P.; Giglio, L.; Csiszar, I. The New VIIRS 375 m active fire detection data product: Algorithm description and initial assessment. *Remote Sensing of Environment* **2014**, *143*, 85–96.
7. Giglio, L.; Schroeder, W.; Justice, C. The collection 6 MODIS active fire detection algorithm and fire products. *Remote sensing of environment* **2016**, *178*, 31 – 41.
8. Xu, W.; Wooster, M.; He, J.; Zhang, T. First study of Sentinel-3 SLSTR active fire detection and FRP retrieval: Night-time algorithm enhancements and global intercomparison to MODIS and VIIRS AF products. *Remote Sensing of Environment* **2020**, *248*, 111947.
9. Oliva, P.; Schroeder, W. Assessment of VIIRS 375 m active fire detection product for direct burned area mapping. *Remote Sensing of Environment* **2015**, *160*, 144–155.
10. Schroeder, W.; Prins, E.; Giglio, L.; Csiszar, I.; Schmidt, C.; Morisette, J.; Morton, D. Validation of GOES and MODIS active fire detection products using ASTER and ETM+ data. *Remote Sensing of Environment* **2008**, *112*, 2711–2726.
11. Li, F.; Zhang, X.; Kondragunta, S. Biomass Burning in Africa: An Investigation of Fire Radiative Power Missed by MODIS Using the 375 m VIIRS Active Fire Product. *Remote. Sens.* **2020**, *12*, 1561.
12. Fu, Y.; Li, R.; Wang, X.; Bergeron, Y.; Valeria, O.; Chavardès, R.D.; Wang, Y.; Hu, J. Fire Detection and Fire Radiative Power in Forests and Low-Biomass Lands in Northeast Asia: MODIS versus VIIRS Fire Products. *Remote. Sens.* **2020**, *12*, 2870.
13. Koltunov, A.; Ustin, S.; Quayle, B.; Schwind, B. EARLY FIRE DETECTION (GOES-EFD) SYSTEM PROTOTYPE. 2012.
14. Koltunov, A.; Ustin, S.L.; Quayle, B.; Schwind, B.; Ambrosia, V.; Li, W. The development and first validation of the GOES Early Fire Detection (GOES-EFD) algorithm. *Remote Sensing of Environment* **2016**, *184*, 436–453.
15. Kotroni, V.; Cartalis, C.; Michaelides, S.; Stoyanova, J.; Tymvios, F.; Bezes, A.; Christoudias, T.; Dafis, S.; Giannakopoulos, C.; Giannaros, T.M.; et al. DISARM Early Warning System for Wildfires in the Eastern Mediterranean. *Sustainability* **2020**, *12*.
16. Schmidt, C.; Hoffman, J.; Prins, E.; Lindstrom, S. GOES-R advanced baseline imager (ABI) algorithm theoretical basis document for fire/hot spot characterization, version 2.0, NOAA, Silver Spring, Md. *NOAA NESDIS, Cent. Satell. Appl. Res* **2010**.

17. Li, F.; Zhang, X.; Kondragunta, S.; Schmidt, C.C.; Holmes, C.D. A preliminary evaluation of GOES-16 active fire product using Landsat-8 and VIIRS active fire data, and ground-based prescribed fire records. *Remote Sensing of Environment* **2020**, *237*, 111600.
18. Hall, J.V.; Zhang, R.; Schroeder, W.; Huang, C.; Giglio, L. Validation of GOES-16 ABI and MSG SEVIRI active fire products. *Int. J. Appl. Earth Obs. Geoinformation* **2019**, *83*.
19. Zhu, X.; Tuia, D.; Mou, L.; Xia, G.S.; Zhang, L.; Xu, F.; Fraundorfer, F. Deep learning in remote sensing: a review. *ArXiv* **2017**, *abs/1710.03959*.
20. Ban, Y.; Zhang, P.; Nascetti, A.; Bevington, A.R.; Wulder, M. Near Real-Time Wildfire Progression Monitoring with Sentinel-1 SAR Time Series and Deep Learning. *Scientific Reports* **2020**, *10*.
21. Mou, L.; Ghamisi, P.; Zhu, X.X. Deep Recurrent Neural Networks for Hyperspectral Image Classification. *IEEE Transactions on Geoscience and Remote Sensing* **2017**, *55*, 3639–3655. doi:10.1109/TGRS.2016.2636241.
22. Toan, N.T.; Phan, T.C.; Hung, N.; Jo, J. A deep learning approach for early wildfire detection from hyperspectral satellite images. *2019 7th International Conference on Robot Intelligence Technology and Applications (RiTA)* **2019**, pp. 38–45.
23. Cho, K.; Merrienboer, B.V.; Çaglar Gülçehre.; Bahdanau, D.; Bougares, F.; Schwenk, H.; Bengio, Y. Learning Phrase Representations using RNN Encoder–Decoder for Statistical Machine Translation. *ArXiv* **2014**, *abs/1406.1078*.
24. Mission Overview [WWW Document], n.d. [WWW Document]. Mission Overview GOES-R Series. In Proceedings of the URL https://www.goes-r.gov/mission/mission.html, (accessed 4.7.21).
25. Barducci, A.; Guzzi, D.; Marcoionni, P.; Pippi, I. Comparison of fire temperature retrieved from SWIR and TIR hyperspectral data. *Infrared Physics Technology* **2004**, *46*, 1–9.
26. Gorelick, N.; Hancher, M.; Dixon, M.; Ilyushchenko, S.; Thau, D.; Moore, R. Google Earth Engine: Planetary-scale geospatial analysis for everyone. *Remote Sensing of Environment* **2017**, *202*, 18–27.
27. Hochreiter, S.; Schmidhuber, J. Long Short-Term Memory. *Neural Computation* **1997**, *9*, 1735–1780.
28. Wang, W.; Yang, N.; Wei, F.; Chang, B.; Zhou, M. Gated Self-Matching Networks for Reading Comprehension and Question Answering. In Proceedings of the ACL, 2017.
29. Lin, T.Y.; Goyal, P.; Girshick, R.B.; He, K.; Dollár, P. Focal Loss for Dense Object Detection. *IEEE Transactions on Pattern Analysis and Machine Intelligence* **2020**, *42*, 318–327.
30. Abadi, M.; Barham, P.; Chen, J.; Chen, Z.; Davis, A.; Dean, J.; Devin, M.; Ghemawat, S.; Irving, G.; Isard, M.; et al. TensorFlow: A system for large-scale machine learning. In Proceedings of the OSDI, 2016.